PCCP

High Level *ab initio* investigation of the Catalytic Effect of Water on Formic Acid Decomposition and Isomerization

Journal:	*Physical Chemistry Chemical Physics*
Manuscript ID	CP-ART-07-2020-003796.R2
Article Type:	Paper
Date Submitted by the Author:	08-Oct-2020
Complete List of Authors:	Wolf, Mark; University of Georgia , Center for Computational Quantum Chemsitry; Turney, Justin; University of Georgia, Center for Computational Chemistry Schaefer, Henry; University of Georgia, Computational Chemistry

PCCP

ARTICLE TYPE

Cite this: DOI: 00.0000/xxxxxxxxxx

High Level ab initio Investigation of the Catalytic Effect of Water on Formic Acid Decomposition and Isomerization†

Mark E. Wolf[a], Justin M. Turney[a], and Henry F. Schaefer III[a*]

Received Date
Accepted Date

DOI: 00.0000/xxxxxxxxxx

Formic acid (FA) is a ubiquitous molecule found in the atmosphere, and it is important to many important processes. The FA molecule generally exists as the *trans* isomer, which can decompose into H_2O and CO (dehydration). It can also exist in the less favorable *cis* isomer which can decompose into H_2 and CO_2 (decarboxylation). Our work examines the complexes formed between each isomer of FA with water. We present geometries and vibrational frequencies obtained at the reliable CCSD(T)/aug-cc-pVTZ level of theory for seven FA$\cdots$water complexes. We utilize the focal point method to determine CCSDT(Q)/CBS plus corrections binding energies of 7.37, 3.36, and 2.02 kcal mol^{-1} plus 6.07, 3.79, 2.60, and 2.55 kcal mol^{-1} for the *trans*-FA$\cdots$water and *cis*-FA$\cdots$water complexes, respectively. Natural bond orbital analysis is used to further decompose the interactions in each complex and gain insight into their relative strengths. Furthermore, we examine the effect that a single water molecule has on the barrier heights to each decomposition pathway by optimizing the transition states and verifying their connectivity with intrinsic reaction coordinate computations and utilizing a kinetic model. Water lowers the barrier to dehydration by at most 15.78 kcal mol^{-1} and the barrier to decarboxylation by up to 15.90 kcal mol^{-1}. Our research also examines for the first time the effect of one water molecule on the interconversion barrier and we find that the barrier from *trans* to *cis* is not catalyzed by water due to the strong FA and water interactions. Our results highlight some instances where different binary complexes result in different decomposition pathways and even a case where one binary complex can form the same decomposition products via two distinct mechanisms. Our results provide a reliable benchmark of the FA$\cdots H_2O$ system as well as provide insight into future studies of similar atmospheric systems.

1 Introduction

Over the past century scientific research has made great progress in understanding the chemistry of earth's atmosphere. Relatively recent realizations of the negative health and environmental effects of atmospheric imbalances has motivated research on scientific, humanitarian, and environmental levels.[1–4] The study of atmospheric organic compounds has been of particular significance to understanding the chemical interworkings of the atmosphere.[5–7] Atmospheric organic compounds existing in the gas phase are suggested to play a central role in the nucleation of atmospheric aerosols via the formation of noncovalent complexes.[8] These aerosols have been shown to affect breathable air quality, earth's radiation budget, the formation of atmospheric ice, and the meteorological behavior of clouds.[9,10] It is an open research question to understand the mechanism for which these organic compound begin to nucleate and how their noncovalent interactions impact chemical reactions that may significantly influence environmental science and human health.

One of the most ubiquitous organic molecules in the earth's atmosphere is formic acid. Formic acid is the simplest carboxylic acid and is thought to be one of the most significant contributors to atmospheric acidity, of central importance to the organic compound oxidation cascade, and a respiratory irritant.[11,12] The primary sources of formic acid in the atmosphere are from the general biomass, natural vegetation, and the burning of fossil- and bio-fuels. Formic acid is also indirectly produced as a product of many atmospheric chemical processes.[13–17] The prevalence and importance of formic acid in the atmosphere is undeniable and easily motivates the study of important chemical pathways related to its formation or decomposition.

Formic acid (HCOOH), henceforth reffered to as FA, exists in either a *cis* or *trans* conformation depending on the orientation of the hydroxyl group.[18] The *cis* conformer is 3.90 kcal mol^{-1} higher in energy than the *trans* conformer, resulting in approximately a 1:800 relative abundance at room temperature.[18,19]

* *Center for Computational Quantum Chemistry, University of Georgia, 140 Cedar Street, Athens, Georgia 30602 United States of America. Fax: (706) 542-0406; Tel: (706) 542-2067; E-mail: ccq@uga.edu*

† Electronic Supplementary Information (ESI) available: [details of any supplementary information available should be included here]. See DOI: 10.1039/cXCP00000x/

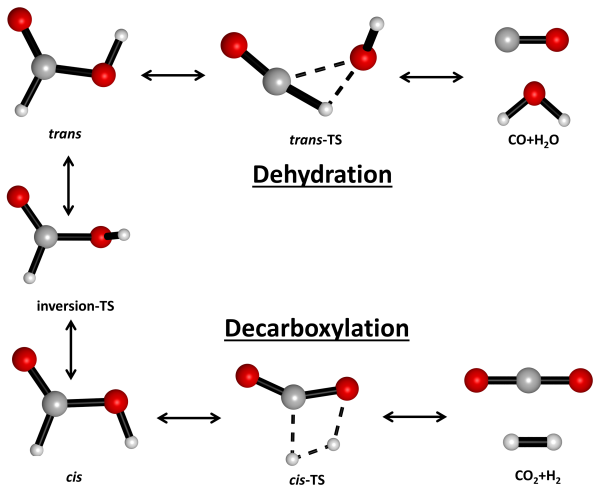

Fig. 1 The two decomposition pathways that formic acid can undergo. The *trans* isomer follows the dehydration pathway and breaks into CO and H_2O, while the *cis* isomer follows the decarboxylation pathway breaking into CO_2 plus H_2. The two isomers are linked by a transition state that interconverts the two.

Because of formic acid's role in the production of acid rain, it is important to understand its decomposition mechanisms. Savage and Akiya noted that the determining factor of a formic acid molecule undergoing either decarboxylation or dehydration (Figure 1) is its proclivity to be in the in the *cis* or *trans* conformation, respectively.[20] The dehydration mechanism has been experimentally shown to be the dominant pathway; however the similar barrier height of the decarboxylation pathway has raised the question why this is the case.[21,22] Hu and coworkers reported theoretical results that indicate formic acid in the presence of H_2 enhances the dehydration pathway significantly relative to the decarboxylation route.[23] They also motivate how important the noncovalent interaction of H_2 is with FA which might have a large influence on the CO/CO_2 product ratio of the reaction. Machado and coworkers recently published theoretical RRKM kinetic results in 2020 that provided evidence that the isomerization reaction is the key step to explaining why the dehydration step is dominant for uncatalyzed decomposition.[21]

Atmospheric conditions often allow for binary complexes to form between various combinations of small molecules including FA. Abundant research has been conducted both theoretically and experimentally to characterize the complexes that FA can form with H_2O[24–27], CO_2[26], SO_2[28], H_2O_2[29], hydroxyl radical[30], hydroperoxyl radical[31], formic acid[32,33], and many other relevant atmospheric molecules.[34–43] Accurate geometric and interaction energy computations of these binary complexes are particularly useful to understand their fundamental molecular interactions. However, a far more interesting question is whether these binary complexes play a catalytic role in the decomposition of FA. Hu and coworkers examined the catalytic influence of H_2 on FA decomposition at the CCSD(T)/6-311++G**//MP2/6-311++G** level of theory and found that the interaction with H_2 is a primary reason for the enhancement of the dehydration pathway. The catalytic effect of water has also been proposed and studied for formic acid decomposition in various theoretical studies.[20,22,44] Two studies have computationally examined the role of multiple water molecules on the selectivity of formic acid decomposition routes.[22,44] Both studies found that the barriers to decarboxylation and dehydration are lowered as the number of water molecules increases which is a reasonable considering that a significant portion of atmospheric water exists as a dimer. For the purposes of our research, we will closely examine the role of a single water molecule on the energetics and kinetics of formic acid decomposition. The Hu study demonstrated that H_2 would hinder the interconversion of FA or enhance the dehydration pathway in certain conformations.[23] This finding indicates that it is critical to study the decomposition and interconversion pathways of all binary complexes between FA and water, which the previously mentioned studies did not include.

The FA$\cdots H_2O$ complexes have been previously studied experimentally and theoretically at various levels of theory. In 1995 Nelander and coworkers determined the vibrational structure of the three *trans*-FA$\cdots H_2O$ complexes.[45] Shortly thereafter, Jorgensen and coworkers computationally optimized the same three structures with two additional *cis* complexes at the B3LYP/6-31+G(d(X+),p) level of theory.[46] Five years later, Bauder and coworkers used rotational spectroscopy to determine the geometric parameters of the lowest energy *trans*-FA$\cdots H_2O$ complex.[25] Zhou and coworkers also studied the FA$\cdots H_2O$ complex, finding the three *trans* complexes as well as three *cis* complexes at the MP2/6-311++G(2d,2p) level of theory.[47] It is interesting to note that the interaction energy for each *cis*-FA$\cdots H_2O$ complex they report is significantly higher than the difference in energy between the *cis* and *trans* conformers of formic acid, increasing the thermodynamic favorability of the *cis* in the presence of water. In 2003 Sander and George perfomed a matrix isolation and *ab initio* (MP2/aug-cc-pVTZ) study on the FA$\cdots H_2O$ complex and found the three previously mentioned *trans*-FA$\cdots H_2O$ complexes but make no comment on any of the *cis* complexes. They highlight that a complex with the strongest interaction energy exists for a cyclic geometry with two hydrogen bonds.[24] In 2007, Rasanen and coworkers studied how hydrogen bonding in the *cis*-FA$\cdots H_2O$ can make the *cis*-FA conformer energetically favorable, if the interaction energy of *cis*-FA$\cdots H_2O$ is significantly larger than the energy difference of the *trans*-FA and *cis*-FA conformers.[27] Further explanation of the bonding nature of these complexes or any new complexes would continue the decades long discussion involving FA$\cdots H_2O$ complexes. The question still remains as to how the various conformers influence the formic acid decomposition pathways.

The uncatalyzed decomposition of formic acid has been well studied by experiment and theory.[48–58] The most most reliable computations on the uncatalyzed decomposition to date appear to be those of Vichietti and coworkers at the CBS//CCSD/cc-pVTZ level of theory.[49] Akiya and Savage, in 1998, published the first theoretical research studying water as a heterogeneous catalyst in the decomposition of FA at the HF/3-21G(d,p) level of theory.[20] They found that a single water molecule lowered the barriers to dehydration and decarboxylation by 11.4 and 19.9 kcal mol^{-1}, respectively. The addition of one water molecule makes the *cis*-

FA-H_2O complex lower in energy than the separated *trans*-FA + H_2O and the barrier to decarboxylation lower than the barrier to dehydration. A related study published in 2008 by Chen and coworkers at the G2M//B3LYP/6-311+G(3df, 2p) level of theory found that the the addition of a water molecule lowered the barrier to dehydration and decarboxylation by 16.9 kcal mol^{-1} and 15.7 kcal mol^{-1}, respectively.[44] From these results, the barrier to decarboxylation is slightly lower by 0.3 kcal mol^{-1}. Chen also studied the addition of one to three water molecules and report that the catalytic effect is greater as more water molecules are included. The most recent theoretical study of this system was published in 2014 by Inaba.[22] He reports complexes at the G4 composite level of theory with up to five molecule water clusters. Inaba found that one water molecule lowers the barriers to dehydration and decarboxylation by 17.36 kcal mol^{-1} and 15.79 kcal mol^{-1}, respectively. This results in a slightly larger barrier to decarboxylation by less than 0.2 kcal mol^{-1}.

Each of these previous studies overlook some critical details that influence the potential impact of their results. First, each study concentrates on demonstrating how additional water molecules continues to lower the activation barriers of FA decomposition. This overlooks the fact that it is more likely for a reaction to occur in the presence of one water molecule or dimer even though it is possible for a water cluster to accumulate around a FA molecule and catalyze its decomposition as a unimolecular process. More importantly, each study only considers one FA$\cdots H_2O$ binary complex for each reaction pathway which may miss some of the effects of different conformers as described by Hu and coworkers.[23] Inadequate consideration is given to how different conformations may result in different pathways and barrier heights. Previous literature also makes no mention of water catalyzed interconversion reactions (between the *cis* and *trans* isomers of formic acid), which might have an influence on their relative abundances as well. In this work, we present reliable decomposition pathways for all possible water catalyzed decarboxylation and dehydration pathways for FA. Our work lays a firm foundation for future research looking at the catalytic effects of noncovalent interactions in systems that form multiple binary complexes.

With the prevalence of water and FA in the atmosphere, it is of supreme importance to understand the interactions and the complexes formed between them. From the aforementioned FA$\cdots H_2O$ studies, we have additional motivation to study the higher energy *cis*-FA$\cdots H_2O$ complexes, that appear significantly more favorable than the dissociated *cis*-FA and H_2O molecules. During our research we performed extensive automated conformer searches in order to find any additional FA$\cdots H_2O$ complexes not previously reported in the literature. We have optimized each geometry at the "gold standard" *ab initio* CCSD(T)/aug-cc-pVTZ level of theory and performed focal point analyses to produce highly reliable CCSDT(Q)/CBS plus corrections interaction energies and barrier heights.

2 Methods

Each structure presented in our research was initially found utilizing the Conformer-Rotomer Ensemble Sampling Tool (CREST) package by Stefan Grimme.[59] CREST uses a combination of molecular dynamics sampling, Z-matrix crossing, and normal mode following to provide an ensemble of candidate structures. Previous literature, our CREST results, and our own "manual" scans provided a rigorous base of candidate structures for which a subset we were able to optimize at a high level of theory. All geometries were optimized at the CCSD(T) level of theory with a Dunning aug-cc-pVTZ basis set to capture long range interactions.[60–64] Harmonic vibrational frequencies were obtained at the same level of theory to confirm the nature of each stationary point as either a minima or a transition state. Both geometry optimizations and harmonic vibrational frequency computations utilized the CFOUR2.0 software.[65] Intrinsic reaction coordinate (IRC) scans were performed on all transition states to ensure proper connectivity of the minima using the software package Psi4.[66]

Highly reliable interaction energies were determined using the focal point analysis method of Allen and coworkers to extrapolate the energy of our computed geometries to the complete basis set limit.[67–72] The aug-cc-pVXZ (X=T,Q,5) Hartree–Fock energies were extrapolated using the three-point formula of Feller (Equation 1).[73] For post-Hartree–Fock, aug-cc-pVXZ (X=Q,5) energies were extrapolated to the CBS limit with the two point formula of Helgaker (Equation 2).[74]

$$E_{HF}(X) = E_{\mathrm{HF}}^{\infty} + ae^{-bX} \quad (1)$$

$$E_{corr}(X) = E_{\mathrm{corr}}^{\infty} + aX^{-3} \quad (2)$$

A series of additive corrections were appended to the CBS energies to account for assumptions made within our previous computations using a combination of the software packages: CFOUR2.0, Psi4, and Molpro 2010.[65,66,75] The zero-point vibrational energy (ZPVE) was added using our harmonic frequencies to account for the vibrational energy of the ground state. This converts all of our stationary point energies to zero kelvin enthalpies. (H_{0K}). A frozen core correction (Δ_{FC}) was included to account for the exclusion of core electrons from post-Hartree–Fock computations. The Δ_{FC} value is defined as the difference between the CCSD(T)/aug-cc-pwCVTZ[76] energy computed with all electrons correlated and the energy computed with the core electrons excluded from the correlation energy. To account for relativistic effects of inner core electrons, a scalar relativistic correction (Δ_{Rel}) was included. Δ_{rel} was computed using the exact two-component one-electron (X2c-1e) relativistic method and was defined as the difference between the energy computed with X2C-1e and without X2C-1e at the CCSD(T)/aug-cc-pCVTZ level of theory.[77] To test for any conical intersections or nearby surface crossings, a diagonal Born–Oppenheimer correction (Δ_{DBOC}) was included at the HF/aug-cc-pVTZ level of theory.[78,79] Finally, CCSDT[80,81] (Δ_{T}) and CCSDT(Q)[82,83] ($\Delta_{\frac{1}{2}(\mathrm{Q})}$) corrections were added to account for higher-order correlation effects. The (Δ_{T}) correction is defined as the difference between a CCSDT and CCSD(T) computation at an aug-cc-pVDZ basis set. The ($\Delta_{\frac{1}{2}(\mathrm{Q})}$) is slightly differ-

ent and is defined as half of the difference between the CCSDT(Q) and CCSDT energies computed using a 6-31+G* basis set.[84–86] The $\frac{1}{2}$ factor on the (Q) correction is to rectify an over compensation of the quadruple excitation description in the perturbation theory. This has been previously noted in the literature[71] and was justified with a small benchmark on the uncatalyzed reactions. The final corrected relative enthalpy for each species is given by Equation 3 relative to the separate water and *trans*-FA molecules.

$$\Delta H_{0K} = \Delta E_{CCSDT/(CBS)} + \Delta_{ZPVE} + \Delta_{FC} + \Delta_{Rel} + \Delta_{DBOC} + \Delta_{\frac{1}{2}(Q)} \quad (3)$$

The noncovalent interactions between water and formic acid were further studied using Natural Bond Orbital analysis utilizing NBO6.0[87,88] as interfaced with the ORCA software package.[89] The NBO computations were all performed using an aug-cc-pVDZ basis set and the B3LYP functional.[90] We present $E^{(2)}$ results (from the NBO computations) which is defined in Equation 4. F_{ij} is the Fock matrix element between i and j natural bond orbitals, ε is the orbital energy and q is the orbital occupation. This value gives an indication of the strength of different NBO orbital overlaps and allows for a clear qualitative interpretation of the bonding interactions.

$$E^{(2)} = q_i[\frac{F_{ij}^2}{\varepsilon_j - \varepsilon_i}] \quad (4)$$

3 Results

3.1 Geometries and Energetics

Each geometry presented has been optimized at the CCSD(T)/aug-cc-pVTZ level of theory. Cartesian coordinates are provided in the supplementary information section along with their respective harmonic vibrational frequencies. The ΔH_{0K} for each stationary point is plotted in Figure 2 and these values are relative to separated *trans*-FA plus water.

The additive corrections overall behaved similarly for each species with a few exceptions. The magnitudes of the ZPVE corrections ranged from 0.22 kcal mol^{-1} to 7.69 kcal mol^{-1}. With the mean around 2.0 kcal mol^{-1} for all binary complexes and 4.0 kcal mol^{-1} for each transition state. The Δ_{FC} and Δ_{Rel} values were small, with the highest magnitude corrections being 0.34 kcal mol^{-1} and 0.17 kcal mol^{-1}, respectively, and much smaller for the vast majority of the stationary points. The DBOC correction was approximately 0.01 kcal mol^{-1} for the majority of stationary points, with a few transition states having a sightly larger DBOC around 0.08 kcal mol^{-1}, not indicative of nearby electronic states. The Δ_T corrections were quite small and never above 0.33 kcal mol^{-1} and usually less than 0.10 kcal mol^{-1} for all of the structures studied. The $\Delta_{\frac{1}{2}(Q)}$ values were slightly larger, but never more than 0.37 kcal mol^{-1} in the worst case scenario. These results give us confidence to make a conservative estimate for our energetic uncertainty to be no more than 1 kcal mol^{-1}.

The natural starting point for the discussion of geometries in this study is to first examine the formic acid structures. Formic acid has two conformers which will be denotes as **Trans** and **Cis** for the monomer species. The **Trans** is named as such because the hydroxyl group is directed opposite from the α-hydrogen with respect to the C-OH bond. If the hydroxyl group is instead oriented towards the α-Hydrogen, the the formic acid is described as the **Cis** and is predicted to lie 4.00 kcal mol^{-1} higher in energy than the **Trans** conformer (Table 1). The two are separated by an interconversion transition state (Labeled **Inter** on Figure 2) 11.53 kcal mol^{-1} higher in energy than the *trans*-FA structure. A more in depth discussion of the interconversion can be found in the section entitled “Interconversions".

Our computations found seven weakly bound noncovalent complexes between water and FA. Three of these complexes contain the *trans* conformer of formic acid and are denoted as, **T1**, **T2**, and **T3**, ordered from lowest to highest energy and can be seen in Figure 3 along with their focal pointed relative energies in Table 2. Each complex involves two interactions between water and two of the three distinct FA functional groups. Likewise, there are four complexes between water and the *cis* conformer of formic acid (**C1**, **C2**, **C3**, **C4**). Each of the *trans* structures along with **C1**, **C2**, and **C4** were previously characterized.[47] However, **C3** is a new FA$\cdots$H$_2$O complex that has not been reported in the literature.

The lowest energy stationary point is **T1** which has a large predicted binding energy of 7.37 kcal mol^{-1}. The most comparable theoretical work to date for the *trans* complexes is from Sander and George.[24] They optimized the three *trans* structures at the MP2/aug-cc-pVTZ level of theory. For **T1**, they reported a ZPVE corrected binding energy of –8.0 kcal mol^{-1}. The strong binding energy is explained by the structure of **T1** which consists of a pair of hydrogen bonds between water and formic acid. The first hydrogen bond exists between a water hydrogen and the carbonyl group and its distance is 2.011 Å, which is 0.009 Å longer than the MP2 values reported by Sander and George. The second bond exists between the hydroxyl group and the oxygen of water, with a distance of 1.785 Å compared to the much shorter MP2 length of 1.768 Å.

The next *trans*-FA$\cdots$water complex is much higher in energy with a binding energy of only 3.36 kcal mol^{-1} which is slightly weaker than the predicted MP2 binding energy of 3.8 kcal mol^{-1}. **T2** is a C_s structure that also features a pair of hydrogen bonds. The first is between a water hydrogen and the carbonyl group, and the second is between the α-hydrogen and the water oxygen. The hydrogen bond with the carbonyl seems to be the dominant interaction with an internuclear separation of 2.013 Å which is 0.01 Å longer then the MP2 value. The hydrogen bond with the α-hydrogen is much longer at 2.564 Å. The structure of **T2** is quite similar to **T1**, but the binding energy of **T2** is likely much smaller because the water molecule is sterically hindered from its most favorable orientation with respect to the second hydrogen bond.

The final *trans* complex, **T3**, is characterized by a C_s geometry and a binding energy of 2.02 kcal mol^{-1}. This is less than the reported MP2 binding energy of 2.5 kcal mol^{-1}. **T3** consists of two interactions between water and *trans*-FA. The first is a hydrogen

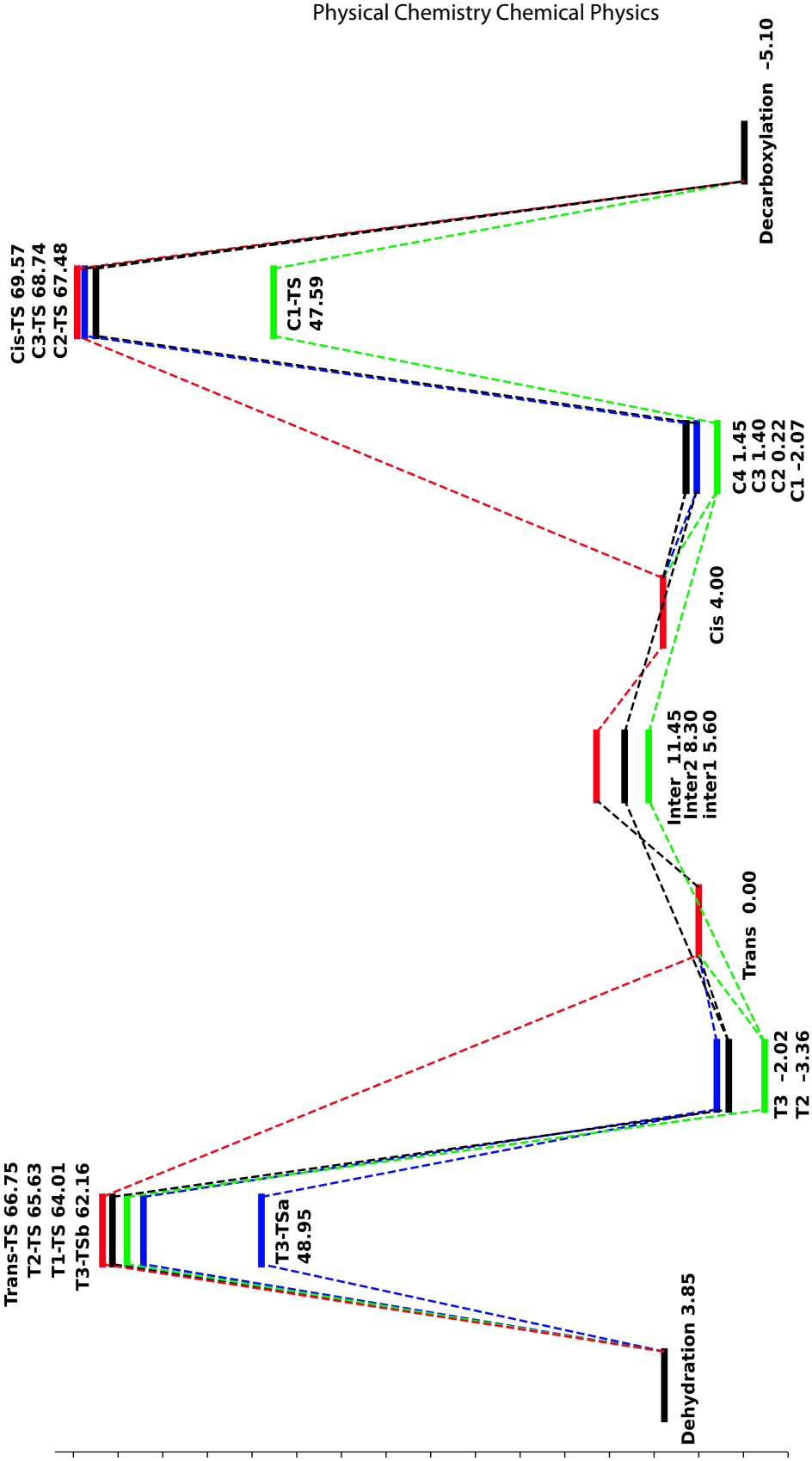

Fig. 2 The ΔH_{0K} for minima and transition states relative to separated *trans*-formic acid plus water in kcal mol^{-1} Different colors are used to highlight the connectivity of species.

cis						
	HF	+δ MP2	+δ CCSD	+δ (T)	+δ T	NET
aug-cc-pVDZ	+4.85	-0.58	–0.02	–0.03	–0.04	[+4.18]
aug-cc-pVTZ	+4.75	–0.51	+0.01	–0.04	[–0.04]	[+4.18]
aug-cc-pVQZ	+4.71	–0.47	+0.02	–0.04	[–0.04]	[+4.18]
aug-cc-pV5Z	+4.71	–0.46	+0.02	–0.04	[–0.04]	[+4.20]
CBS LIMIT	[+4.72]	[–0.44]	[+0.02]	[–0.04]	[–0.04]	[+4.22]
$E_{CCSDT/CBS+\Delta}$ =4.22–0.22 –0.00–0.00+0.00+0.01 = **4.00**						
Inter						
	HF	+δ MP2	+δ CCSD	+δ (T)	+δ T	NET
aug-cc-pVDZ	+12.28	+0.77	–0.77	+0.22	–0.02	[+12.48]
aug-cc-pVTZ	+12.15	+0.82	–0.71	+0.24	[–0.02]	[+12.48]
aug-cc-pVQZ	+12.16	+0.89	–0.69	+0.24	[–0.02]	[+12.58]
aug-cc-pV5Z	+12.17	+0.92	–0.69	+0.24	[–0.02]	[+12.62]
CBS LIMIT	[+12.17]	[+0.96]	[–0.69]	[+0.24]	[–0.02]	[+12.66]
$E_{CCSDT/CBS+\Delta}$ =12.66–1.25+0.01+0.01+0.01+0.01= **11.45**						
***cis*-TS**						
	HF	+δ MP2	+δ CCSD	+δ (T)	+δ T	NET
aug-cc-pVDZ	+93.05	–19.79	+5.99	–3.63	–0.00	[+75.62]
aug-cc-pVTZ	+92.65	–19.63	+6.50	–3.98	[–0.00]	[+75.53]
aug-cc-pVQZ	+92.62	–19.53	+6.63	–4.05	[–0.00]	[+75.67]
aug-cc-pV5Z	+92.65	–19.51	+6.65	–4.07	[–0.00]	[+75.72]
CBS LIMIT	[+92.67]	[–19.48]	[+6.68]	[–4.10]	[–0.00]	[+75.77]
$E_{CCSDT/CBS+\Delta}$ =75.77 –6.16 –0.18+ 0.15 –0.10+0.09= **69.57**						
***trans*-TS**						
	HF	+δ MP2	+δ CCSD	+δ (T)	+δ T	NET
aug-cc-pVDZ	+87.06	–20.11	+5.71	–3.86	–0.11	[+68.69]
aug-cc-pVTZ	+88.29	–19.31	+6.38	–4.25	[–0.11]	[+71.00]
aug-cc-pVQZ	+88.42	–19.14	+6.64	–4.31	[–0.11]	[+71.50]
aug-cc-pV5Z	+88.47	–19.01	+6.73	–4.33	[–0.11]	[+71.75]
CBS LIMIT	[+88.50]	[–18.88]	[+6.82]	[–4.36]	[–0.11]	[+71.98]
$E_{CCSDT/CBS+\Delta}$ =71.98–5.03–0.33+0.29–0.16–0.00 = **66.75**						
CO_2 +H_2						
	HF	+δ MP2	+δ CCSD	+δ (T)	+δ T	NET
aug-cc-pVDZ	+87.06	–20.11	+5.71	–3.86	–0.11	[+68.69]
aug-cc-pVTZ	+88.29	–19.31	+6.38	–4.25	[–0.11]	[+71.00]
aug-cc-pVQZ	+88.42	–19.14	+6.64	–4.31	[–0.11]	[+71.50]
aug-cc-pV5Z	+88.47	–19.01	+6.73	–4.33	[–0.11]	[+71.75]
CBS LIMIT	[+88.50]	[–18.88]	[+6.82]	[–4.36]	[–0.11]	[+71.98]
$E_{CCSDT/CBS+\Delta}$ =71.98–7.69–0.00–0.05–0.11+0.02 = **–5.10**						
CO +H_2O						
	HF	+δ MP2	+δ CCSD	+δ (T)	+δ T	NET
aug-cc-pVDZ	+1.19	+5.62	–2.59	+0.86	–0.17	[+4.91]
aug-cc-pVTZ	+1.88	+7.76	–2.27	+0.95	[–0.17]	[+8.14]
aug-cc-pVQZ	+1.59	+8.23	–2.20	+1.00	[–0.17]	[+8.45]
aug-cc-pV5Z	+1.57	+8.36	–2.19	+1.01	[–0.17]	[+8.58]
CBS LIMIT	[+1.59]	[+8.49]	[–2.17]	[+1.02]	[–0.17]	[+8.75]
$E_{CCSDT/CBS+\Delta}$ =8.75+3.07–0.35+0.35–0.17–0.01 = **3.85**						

Table 1 Focal point results for all reactants and products of the uncatalyzed decomposition reactions. The bold energy values are the $\Delta H_{0K} = \Delta E_{CCSDT/(CBS)} + \Delta_{ZPVE} + \Delta_{FC} + \Delta_{.5(Q)} + \Delta_{Rel} + \Delta_{DBOC}$ energies relative to *trans*-FA plus H_2O. See the Methods section for detailed descriptions of these additive corrections.

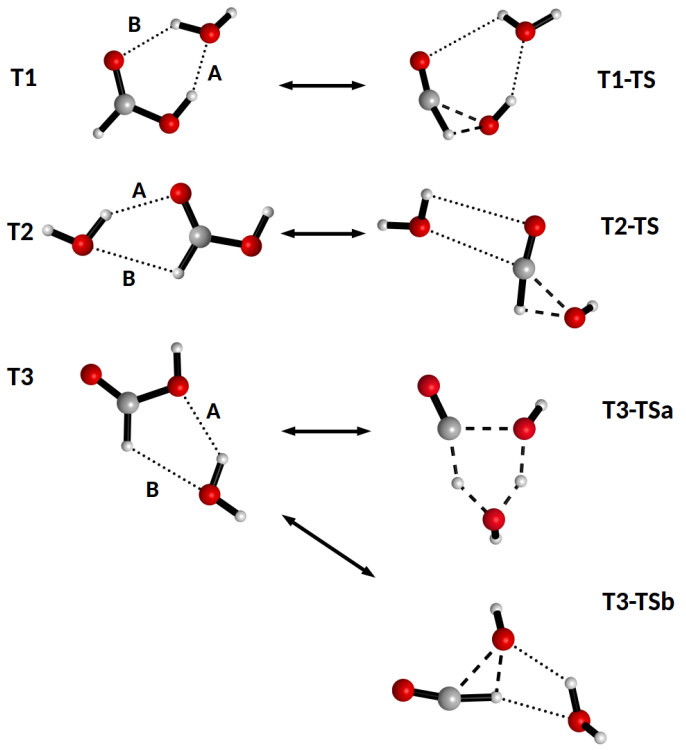

Fig. 3 *Trans* structures and the corresponding dehydration transition states. The dominant noncovalent interactions are labeled A and B for each complex, with A having the stronger bonding character of the two.

bond between a water hydrogen and the hydroxyl group exhibiting a length of 2.181 Å, 0.012 Å larger than the MP2 value. The second, is an interaction between the α-hydrogen and the oxygen of water with a length of 2.463 Å which is shorter than the MP2 result by 0.015 Å.

There are four complexes formed between *cis* formic acid and water which can be seen with their corresponding transition states in Figure 4 along with their focal pointed relative energies in Table 2. The first three have been previously reported in the literature, but the third is a novel result of our computations. The most reliable computations to date for the *cis* complexes are from a theoretical study of Zhou and coworkers, who optimized geometries at the MP2/6-311++g(d,p) level of theory and further refined the resulting energies with CCSD(T) single point computations. However, they did not include zero point vibrational energy corrections, so we can only make comparisons to the geometries they present. The lowest energy *cis* structure, **C1**, has a binding energy of 6.07 kcal mol^{-1}. The structure has C_s symmetry with a single hydrogen between the hydroxyl group and the oxygen of water. The bond length that we compute is 1.815 Å which is very close to the MP2 distance of 1.817 Å.

Slightly higher in energy is the **C2** complex which has a binding energy of 3.79 kcal mol^{-1}. **C2** also has a planar geometry which exhibits two weak interactions between the formic acid and water. First is a hydrogen bond between the water hydrogen atom and the carbonyl. The second is an interaction between the water oxygen and the α-hydrogen. The distances associated with these

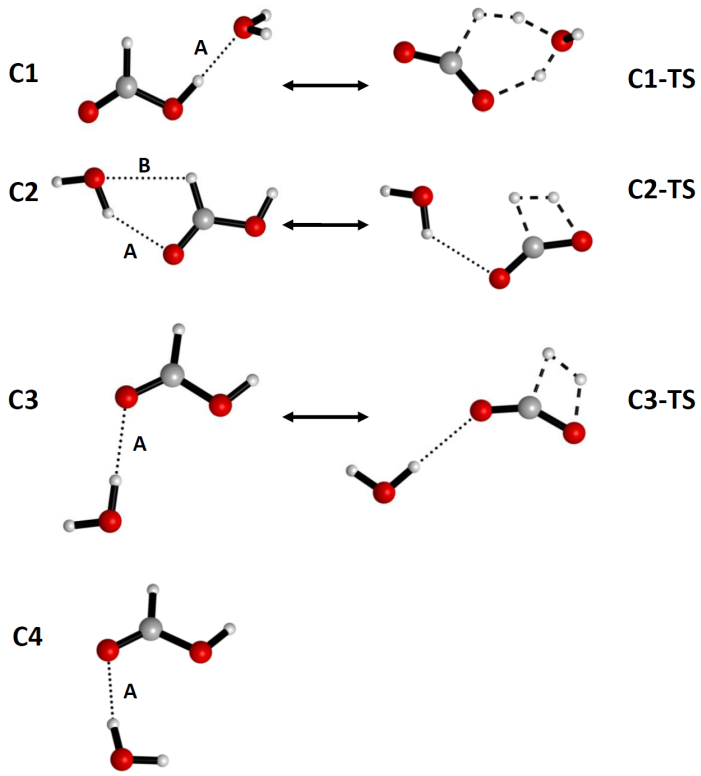

Fig. 4 *Cis* structures and their corresponding decarboxylation transition states. The dominant noncovalent interactions are labeled A and B for each complex, with A being the stronger of the two.

interactions are 2.008 Å and 2.508 Å, respectively. The hydrogen bond we report is over 0.05 Å shorter than the previously reported MP2 distance.

The final two complexes are closely related. Both **C3** and **C4** contain a single hydrogen bond between the hydrogen of water and the carbonyl. Each geometry exhibits C_s symmetry with the the only difference being the orientation of the non-interacting water hydrogen atom pointed towards the hydroxyl oxygen (**C3**) or away from the FA molecule (**C4**). The former complex has not previously been reported in the literature. The predicted binding energies for **C3** and **C4** are 2.60 and 2.55 kcal mol^{-1}, respectively. This correlates with the length of the hydrogen bonds for which **C4** is 0.0305 Å longer.

Natural bond orbital (NBO) Analysis is a helpful tool to understand the nature of the noncovalent interactions in each of the binary complexes presented. Table 3 presents the dominant contributions to the second order perturbation interaction energy ($E^{(2)}$) between water and formic acid in each complex. These values estimate the energetic importance of each interaction between all donor and acceptor NBOs by means of second order perturbation theory. It is key to note that these estimates are not quantitative predictions of the actual interaction energy, but instead provides a means for qualitative comparisons between between different NBO interactions. The dominant interaction is labeled with an A and the weaker secondary interaction is labeled with a B, as depicted in Figures 3 and 4. It should be noted that the $E^{(2)}$ values

T1

	HF	+δ MP2	+δ CCSD	+δ (T)	+δ T	NET
aug-cc-pVDZ	–6.99	–3.51	+0.72	–0.73	+0.02	[–10.49]
aug-cc-pVTZ	–6.62	–3.94	+0.72	–0.75	[+0.02]	[–10.57]
aug-cc-pVQZ	–6.56	–3.94	+0.76	–0.76	[+0.02]	[–10.47]
aug-cc-pV5Z	–6.50	–3.90	+0.77	–0.76	[+0.02]	[–10.36]
CBS LIMIT	[–6.47]	[–3.87]	[+0.78]	[–0.76]	[+0.02]	[–10.28]

$E_{CCSDT/CBS+\Delta}$ =–10.28+2.61 +0.35–0.05+0.03–0.03 = **–7.37**

T2

	HF	+δ MP2	+δ CCSD	+δ (T)	+δ T	NET
aug-cc-pVDZ	–4.14	–1.62	+0.22	–0.32	+0.02	[–5.84]
aug-cc-pVTZ	–3.67	–1.88	+0.21	–0.33	[+0.02]	[–5.64]
aug-cc-pVQZ	–3.63	–1.84	+0.24	–0.33	[+0.02]	[–5.54]
aug-cc-pV5Z	–3.61	–1.81	+0.25	–0.32	[+0.02]	[–5.47]
CBS LIMIT	[–3.59]	[–1.77]	[+0.25]	[–0.32]	[+0.02]	[–5.41]

$E_{CCSDT/CBS+\Delta}$ = –5.41+1.72+0.36–0.03+0.02–0.02 = **–3.36**

T3

	HF	+δ MP2	+δ CCSD	+δ (T)	+δ T	NET
aug-cc-pVDZ	–2.31	–1.72	+0.17	–0.27	+0.01	[–4.13]
aug-cc-pVTZ	–1.91	–1.88	+0.17	–0.28	[+0.01]	[–3.89]
aug-cc-pVQZ	–1.86	–1.84	+0.20	–0.28	[+0.01]	[–3.77]
aug-cc-pV5Z	–1.84	–1.79	+0.20	–0.28	[+0.01]	[–3.70]
CBS LIMIT	[–1.82]	[–1.75]	[+0.20]	[–0.28]	[+0.01]	[–3.64]

$E_{CCSDT/CBS+\Delta}$ =–3.64+1.29+0.35 –0.02–+0.01–0.01 = **–2.02**

C1

	HF	+δ MP2	+δ CCSD	+δ (T)	+δ T	NET
aug-cc-pVDZ	–2.05	–2.33	+0.37	–0.40	–0.00	[–4.41]
aug-cc-pVTZ	–1.96	–2.37	+0.36	–0.38	[–0.00]	[–4.34]
aug-cc-pVQZ	–1.92	–2.27	+0.40	–0.38	[–0.00]	[–4.17]
aug-cc-pV5Z	–1.88	–2.22	+0.40	–0.37	[–0.00]	[–4.07]
CBS LIMIT	[–1.85]	[–2.17]	[+0.41]	[–0.37]	[–0.00]	[–3.99]

$E_{CCSDT/CBS+\Delta}$ =–3.99+1.60+0.35 –0.05+0.03–0.02 = **–2.07**

C2

	HF	+δ MP2	+δ CCSD	+δ (T)	+δ T	NET
aug-cc-pVDZ	+0.13	–2.20	+0.23	–0.35	–0.02	[–2.21]
aug-cc-pVTZ	+0.55	–2.42	+0.25	–0.37	[–0.02]	[–2.01]
aug-cc-pVQZ	+0.55	–2.37	+0.29	–0.37	[–0.02]	[–1.91]
aug-cc-pV5Z	+0.58	–2.31	+0.29	–0.37	[–0.02]	[–1.83]
CBS LIMIT	[+0.60	[–2.26]	[+0.29]	[–0.37	[–0.02]	[–1.75]

$E_{CCSDT/CBS+\Delta}$ =–1.75+1.61 +0.38 –0.03+0.02–0.01= **0.22**

C3

	HF	+δ MP2	+δ CCSD	+δ (T)	+δ T	NET
aug-cc-pVDZ	+1.26	–1.76	+0.17	–0.29	–0.02	[–0.64]
aug-cc-pVTZ	+1.37	–1.80	+0.19	–0.29	[–0.02]	[–0.55]
aug-cc-pVQZ	+1.35	–1.69	+0.22	–0.29	[–0.02]	[–0.43]
aug-cc-pV5Z	+1.38	–1.64	+0.22	–0.28	[–0.02]	[–0.35]
CBS LIMIT	[+1.40]	[–1.59]	[+0.23]	[–0.28]	[–0.02]	[–0.27]

$E_{CCSDT/CBS+\Delta}$ =–0.27+1.32 +0.36–0.03+0.01–0.00 = **1.40**

C4

	HF	+δ MP2	+δ CCSD	+δ (T)	+δ T	NET
aug-cc-pVDZ	+1.60	–1.97	+0.17	–0.32	–0.02	[–0.55]
aug-cc-pVTZ	+1.77	–2.06	+0.20	–0.33	[–0.02]	[–0.45]
aug-cc-pVQZ	+1.76	–1.97	+0.23	–0.33	[–0.02]	[–0.34]
aug-cc-pV5Z	+1.79	–1.92	+0.24	–0.33	[–0.02]	[–0.25]
CBS LIMIT	[+1.81]	[–1.87]	[+0.24]	[–0.33]	[–0.02]	[–0.17]

$E_{CCSDT/CBS+\Delta}$ = –0.17+1.28 +0.36–0.02+0.01–0.00= **1.45**

Table 2 Focal point results for all $H_2O\cdots$FA complex minima. The bold energy values are the $\Delta H_{0K} = \Delta E_{CCSDT/(CBS)} + \Delta_{ZPVE} + \Delta_{FC} + \Delta_{.5(Q)} + \Delta_{Rel} + \Delta_{DBOC}$ energies relative separated *trans*-FA plus H_2O. See the Methods section for detailed descriptions of these additive corrections.

Complex	Distance A	Distance B	$E^{(2)}_{A}$	$E^{(2)}_{B}$	$E^{(2)}_{Total}$	CCSDT(Q)/CBS E_{Int}
T1	1.785	2.011	18.5	5.6	24.1	7.37
T2	2.013	2.564	5.4	0.5	5.9	3.36
T3	2.181	2.463	1.7	1.2	2.9	2.02
C1	1.815		16.4		16.4	6.07
C2	2.008	2.508	5.6	0.7	6.3	3.79
C3	2.012		2.5		2.5	2.60
C4	2.047		4.0		4.0	2.55

Table 3 Relevant information (Å, kcal mol^{-1}) for each noncovalent interaction exhibited by the seven $H_2O\cdots$FA complexes. For complexes with two interactions, the stronger interaction is labeled A and the weaker B, which are shown in Figures 3 and 4. The first two columns are the interaction bond lengths in Å. The next three columns are the second-order perturbation energy ($E^{(2)}$) for the dominant NBO orbital overlap in kcal mol^{-1} for interaction A, B, and the total, respectively. The final column is the interaction energy computed from our focal point method in kcal mol^{-1}.

correlate well with the interaction energies from our focal point analysis. The only exception is **C3** and **C4**, which is understandable given their close CCSDT(Q)/CBS energies and the qualitative nature of the NBO analysis.

The **T1** complex has a significantly stronger binding energy than the other complexes. The most obvious explanation for this is the existence of two strong hydrogen bonds with $E^{(2)}$ values of 18.5 and 5.6 kcal mol^{-1} for interactions A and B, respectively. We are confident that each interaction is a hydrogen bond, since in each case they exhibit donation from a lone pair of oxygen into an antibonding O-H orbitals ($n_O \rightarrow \sigma*_{OH}$). For comparison, just the weak hydrogen bond of **T1** is larger than the strongest interaction of **T2** and almost larger then the sum of both interactions in **T2**. According to the NBO analysis, only the A interaction is significant in **T2** and the contribution of the second hydrogen bond is negligible with a $E^{(2)}$ of only 0.5 kcal mol^{-1}. This is likely due to the fact that water oxygen is now trying to interact with a hydrogen that is far more geometricly constrained relative to the rather flexible hydroxyl hydrogen. The last complex, **T3**, consists of two very weak hydrogen bond interactions of 1.7 and 1.2 kcal mol^{-1} which result in the smallest total interaction energy of the three *trans* structures.

The *cis* complexes present a much simpler NBO analysis with all complexes consisting of a single interaction except for **C2**. In each case, the nature of the orbital donation is again a hydrogen bond characterized by a $n_O \rightarrow \sigma*_{OH}$ interaction. The strongest interaction energy belongs to the single hydrogen bond of **C1** with an $E^{(2)}$ value of 16.4 kcal mol^{-1} which, unsurprisingly, has the shortest hydrogen bond distance of 0.193 Å for all of the *cis* complexes. **C2**, despite being a complex with two noncovalent interactions, only has a total $E^{(2)}$ of 6.3 kcal mol^{-1}. The dominant hydrogen bond, to the carbonyl group, is the primary component with an $E^{(2)}$ value of 5.6 kcal mol^{-1}. The final two structures are closely related and have the weakest hydrogen bonds with $E^{(2)}$ values of 2.5 and 4.0 kcal mol^{-1} for **C3** and **C4**, respectivley. Note that these two structures do not correspond to the order predicted by the coupled cluster results, but this is unsurprising because the CCSDT(Q)/CBS energies are within 0.15 kcal mol^{-1} of each other and the NBO results are not that precise.

To provide some insight into how entropic considerations might effect these systems, and additive Gibbs free energy correction was calculated for each structure from the harmonic vibrational frequency results at 200 K and are presented in the ESI. The Gibbs free energy corrections were at least 3 kcal mol^{-1} for all binary complexes resulting in only **T1** and **C1** predicted as favorable complexes relative to separated FA and water. This does not negate the importance of the other complexes, but emphasizes that they may not be detectable in an appreciable concentration at 200 K. However, the less favorable complexes could still influence FA decomposition and would become increasingly relevant at even lower temperatures.

3.2 Dissociation Pathways

One of the principle findings of this study is that the the different noncovalent complexes formed between formic acid and water can have a significant influence on the catalytic effect for the decarboxylation or dehydrogenation pathways. Previous research has shown that one or more water molecules can greatly lower the barrier to either pathway. However, these studies did not consider how different conformers of formic and water may play a role in this process. All of the complexes discussed in the previous section are significantly lower in energy than separated water and the respective FA isomer, indicating that they are all reasonable catalyzed pathways that may influence the selectivity of the dehydration or decarboxylation pathway. The CCSDT(Q)/CBS relative enthalpies for each water catalyzed decomposition transition state is presented in Table 4.

The dissociation pathways of the *cis* and *trans*-FA monomers has been well characterized. Figure 1 presents the transition states of each pathway. The dehydration pathway is experimentally thought to be the dominant pathway. and proceeds through a transition state that breaks symmetry as the hydroxyl group bends out of the plane of the molecule and begins to abstract the alpha hydrogen to form H_2O and CO. At the CCSD(T)/aug-cc-pVTZ level of theory, this process has a harmonic frequency mode of 1680i cm^{-1} and a barrier height of 66.75 kcal mol^{-1}. The *cis*-FA molecule can undergo a concerted dissociation into CO_2 and H_2 via a C_s transition state with a vibrational mode of 2264i cm^{-1} and a barrier height of 69.57 kcal mol^{-1}. One more key pathway to consider is the rotational barrier of the hydroxyl group that allows for interconversion between the two species. The transition state is also shown in Figure 1 and has a vibrational mode of 600i cm^{-1} and a barrier of 11.45 kcal mol^{-1}. The high interconversion barrier is a primary reason for the observed dominance of the dehydration pathway.

One of the motivating points of this paper is to understand how the inclusion of water affects the barrier heights for the transition states of the complexes relative to the formic acid molecule. This is best expressed by the change in the barrier height (ΔBH) value, which is defined in Equation 5. This will be extremely relevant to the kinetic results that will be discussed later. It is important to note that ΔBH is the result of two competing effects. The first is that the presence of the water molecule lowers the energy of the transition state as expected. At the same time, the water molecule interacts quite strongly with formic acid such that the complex is

T1-TS						
	HF	+δ MP2	+δ CCSD	+δ (T)	+δ T	NET
aug-cc-pVDZ	+85.78	–23.81	+6.28	–4.60	–0.07	[+63.57]
aug-cc-pVTZ	+87.31	–23.37	+7.00	–5.00	[–0.07]	[+65.87]
aug-cc-pVQZ	+87.51	–23.15	+7.29	–5.07	[–0.07]	[+66.51]
aug-cc-pV5Z	+87.60	–23.00	+7.39	–5.09	[–0.07]	[+66.83]
CBS LIMIT	[+87.65]	[–22.83]	[+7.49]	[–5.12]	[–0.07]	[+67.12]
$E_{CCSDT/CBS+\Delta}$ = 67.12–3.24+0.00 +0.28–0.14–0.03= **64.01**						

T2-TS						
	HF	+δ MP2	+δ CCSD	+δ (T)	+δ T	NET
aug-cc-pVDZ	+84.69	–20.17	+5.51	–3.96	–0.10	[+65.97]
aug-cc-pVTZ	+86.20	–19.35	+6.17	–4.33	[–0.10]	[+68.60]
aug-cc-pVQZ	+86.36	–19.14	+6.43	–4.38	[–0.10]	[+69.17]
aug-cc-pV5Z	+86.43	–18.99	+6.52	–4.40	[–0.10]	[+69.47]
CBS LIMIT	[+86.47]	[–18.82]	[+6.61]	[–4.42]	[–0.10]	[+69.74]
$E_{CCSDT/CBS+\Delta}$ = 69.74–4.28+0.03 +0.29–0.15–0.00= **65.63**						

T3-TSa						
	HF	+δ MP2	+δ CCSD	+δ (T)	+δ T	NET
aug-cc-pVDZ	+70.97	–24.53	+6.09	–4.17	–0.03	[+48.34]
aug-cc-pVTZ	+72.47	–24.45	+6.71	–4.56	[–0.03]	[+50.15]
aug-cc-pVQZ	+72.89	–24.20	+7.01	–4.64	[–0.03]	[+51.04]
aug-cc-pV5Z	+73.02	–23.98	+7.09	–4.65	[–0.03]	[+51.45]
CBS LIMIT	[+73.08]	[–23.75]	[+7.17]	[–4.67]	[–0.03]	[+51.80]
$E_{CCSDT/CBS+\Delta}$ = 51.80–3.08+0.26+0.15–0.12–0.06 = **48.95**						

T3-TSb						
	HF	+δ MP2	+δ CCSD	+δ (T)	+δ T	NET
aug-cc-pVDZ	+80.64	–21.06	+5.65	–4.08	–0.10	[+61.04]
aug-cc-pVTZ	+82.38	–20.41	+6.30	–4.44	[–0.10]	[+63.72]
aug-cc-pVQZ	+82.53	–20.08	+6.59	–4.49	[–0.10]	[+64.45]
aug-cc-pV5Z	+82.63	–19.89	+6.69	–4.51	[–0.10]	[+64.81]
CBS LIMIT	[+82.68]	[–19.69]	[+6.78]	[–4.52]	[–0.10]	[+65.15]
$E_{CCSDT/CBS+\Delta}$ =65.15–3.10+0.04+0.25–0.14–0.03 = **62.16**						

C1-TS						
	HF	+δ MP2	+δ CCSD	+δ (T)	+δ T	NET
aug-cc-pVDZ	+70.33	–23.60	+7.02	–4.53	+0.10	[+49.31]
aug-cc-pVTZ	+70.33	–23.77	+7.46	–4.88	[+0.10]	[+49.23]
aug-cc-pVQZ	+70.46	–23.70	+7.62	–4.97	[+0.10]	[+49.51]
aug-cc-pV5Z	+70.56	–23.60	+7.64	–4.99	[+0.10]	[+49.71]
CBS LIMIT	[+70.61]	[–23.48]	[+7.66]	[–5.02]	[+0.10]	[+49.87]
$E_{CCSDT/CBS+\Delta}$ =49.87–2.47 +0.16 +0.05–0.04+0.03= **47.59**						

C2-TS						
	HF	+δ MP2	+δ CCSD	+δ (T)	+δ T	NET
aug-cc-pVDZ	+90.47	–21.60	+6.25	–3.91	+0.03	[+71.24]
aug-cc-pVTZ	+90.60	–21.81	+6.76	–4.27	[+0.03]	[+71.30]
aug-cc-pVQZ	+90.64	–21.73	+6.92	–4.34	[+0.03]	[+71.52]
aug-cc-pV5Z	+90.70	–21.69	+6.95	–4.36	[+0.03]	[+71.63]
CBS LIMIT	[+90.74]	[–21.64]	[+6.99]	[–4.39]	[+0.03]	[+71.72]
$E_{CCSDT/CBS+\Delta}$ = 71.72–4.52+0.17 =+0.12–0.08+0.06= **67.48**						

C3-TS						
	HF	+δ MP2	+δ CCSD	+δ (T)	+δ T	NET
aug-cc-pVDZ	+91.37	–20.55	+6.08	–3.79	+0.01	[+73.12]
aug-cc-pVTZ	+91.08	–20.51	+6.57	–4.12	[+0.01]	[+73.03]
aug-cc-pVQZ	+91.10	–20.33	+6.71	–4.18	[+0.01]	[+73.31]
aug-cc-pV5Z	+91.15	–20.27	+6.74	–4.20	[+0.01]	[+73.43]
CBS LIMIT	[+91.19]	[–20.20]	[+6.77]	[–4.22]	[+0.01]	[+73.54]
$E_{CCSDT/CBS+\Delta}$ = 73.54–5.10+0.18+0.13–0.09+0.08 = **68.74**						

Table 4 Focal point analysis for all $H_2O\cdots FA$ dissociation transition states. The bold energy values are the $\Delta H_{0K} = \Delta E_{CCSDT/(CBS)} + \Delta_{ZPVE} + \Delta_{FC} + \Delta_{.5(Q)} + \Delta_{Rel} + \Delta_{DBOC}$ energies relative to *trans*-FA plus H_2O in kcal mol^{-1}. See the Methods section for the detailed description of these additive corrections.

Complex	$E^{Complex}_{interaction}$	$E^{TS}_{complex} - E^{TS}_{uncatalyzed}$	Barrier Height	ΔBarrier Height
T1-TS	7.37	–2.74	71.38	4.63
T2-TS	3.36	–1.12	68.99	2.24
T3-TSa	2.02	–17.80	48.95	–15.78
T3-TSb	2.02	–4.59	64.18	–2.57
C1-TS	6.07	–21.97	49.66	–15.90
C2-TS	3.79	–2.08	67.27	1.70
C3-TS	2.60	–0.83	67.34	1.77

Table 5 Relevant information (kcal mol^{-1}) for the transition states pertaining to the dehydration and decarboxylation mechanisms for each $H_2O\cdots FA$ complex at the CCSDT(Q)/CBS plus corrections level of theory. The first column is the interaction energy of the minima complexes. The second columns is the difference of the energy of the water catalyzed transition state and the energy of the uncatalyzed transition state. The third column is the barrier height followed by the fourth column which shows the change in the barrier height relative to the uncatalyzed decomposition barrier height.

much lower in energy than the separated formic acid and water molecules. The sum of these values will result in ΔBH and provide insight into why the barrier height is lowered or raised in each case. All results are summarized for each transition state in Table 5. The following sections provide an in depth analysis of the catalytic effects of a water molecule to these processes. Such results may provide insight into the selectivity of each pathway.

$$\Delta BH = BH_{\text{water catalyzed}} - BH_{\text{uncatalyzed}} \quad (5)$$

3.3 Dehydration

Each of the *trans* minima is able to follow the same dehydration reaction mechanism that would otherwise occur with the uncatalyzed decomposition of *trans*-FA. Let us begin with **T1-TS**, which has a vibrational mode of 1749*i* cm^{-1}. We compute a ΔBH of 4.63 kcal mol^{-1} which is primarily the result of a huge interaction energy of the initial complex (7.37 kcal mol^{-1}). The water molecule does significantly lower the transition state energy by 2.47 kcal mol^{-1}, as it is directly interacts with the hydroxyl group during the decomposition, but it is not enough to overcome the two hydrogen bonds formed in **T1**.

The results are similar for **T2-TS**, but with much smaller magnitude. **T2-TS** has a vibrational mode of 1644*i* cm^{-1}. **T2-TS** was difficult to optimize and as a consequence has a second negligible vibrational mode of 31*i* cm^{-1} because the CCSD(T)/aug-cc-pVTZ surface is likely very shallow. **C2-TS** was also found to have a small imaginary mode, but a relaxed optimization found such a small mode inconsequential to the energy or geometry of our system. The ΔBH for **T2-TS**, 2.24 kcal mol^{-1}, is about half the ΔBH for **T1-TS**. The interaction energy of **T2** is still significant at 3.36 kcal mol^{-1}, but **T2-TS** is only 1.12 kcal mol^{-1} lower in energy than **Trans-TS**. This is no surprise as the water molecule is interacting with the carbonyl group, which has little to do with the active site of the transition state.

The **T3** complex can proceed through both the standard dehydration mechanism (**T3-TSb**) discussed above and an alternate mechanism (**T3-TSa**) to from the same products. **T3-TSb** is the only pathway to lower the barrier height of the standard

dehydration pathway relative to **Trans-TS** with a ΔBH value of –2.75 kcal mol^{-1}. **T3-TSb** is characterized by a vibrational mode of 1556*i* cm^{-1} and a barrier height of 64.18 kcal mol^{-1}. **T3** has the weakest interaction of the three binary complexes, giving it more energy as a starting point. The water molecule is positioned to interact with the hydroxyl group and the α-hydrogen, which gives it greater influence on active site of the transition state. **T3-TSa** is completely different with a larger imaginary mode of 1702*i* cm^{-1} as the water and formic acid molecules form a five membered ring that greatly lowers the barrier by 15.78 kcal mol^{-1} relative to **Trans-TS** resulting in a barrier height of 50.97 kcal mol^{-1}. Studies by Inaba and Chen and coworkers presented a barrier height of 48.81 kcal mol^{-1} at the B3LYP/6-311+G(3df, 2p)//G2M(CC1) and 47.5 kcal mol^{-1} at the Gaussian 4 level of theory, respectively for this mechanism.[22,44] This is an extremely interesting result and highlights the fact that there is not necessarily a one to one correspondence between decomposition pathways and noncovalent complexes that still produce the same products. In this case, it is quite important to characterize both as the difference between the transition states is over 13 kcal mol^{-1}.

3.4 Decarboxylation

Transition states for the decarboxylation were found for the first three *cis* complexes, but none could be found for **C4**, despite extensive scans. In contrast to the dehydration transition states in which the complexes can follow the same dehydration mechanism as the uncatalyzed reaction, **C1-TS** deviates from the mechanism that **Cis-Ts** follows. First, we will discuss the other two complexes that do proceed through the expected pathway.

In both cases, **C2-TS** and **C3-TS** increase the barrier height to decarboxylation relative to the uncatalyzed case. They exhibit C_s geometries that proceed through a vibrational modes of 2176*i* cm^{-1} and 2246*i* cm^{-1}, respectively. The potential energy surface for **C3-TS** is extremely shallow and resulted in a vibrational mode of 14*i* cm^{-1} corresponding to a symmetry breaking mode. Symmetry was relaxed and the transition state was re-optimized to remove this second mode and the results were negligible to both the energy and geometry, thus we present the final **C3-TS** structure as C_s. The **C2-TS** and **C3-TS** transition states both have a positive ΔBH, but have the smallest change of any complex (1.70 and 1.77 kcal mol^{-1},respectively). The **C2-TS** ΔBH is small because the lone pair from water interacts with the dissociating H_2 and the **C3-TS** ΔBH is small because it has one of the smallest binding energies of all the complexes.

The **C1-TS** transition state does correspond to a decarboxylation process, but is of a different sort than the others presented thus far. This is easily noticed by its vibrational mode of 1513*i* cm^{-1} which is much smaller then the vibrational mode of 2264*i* cm^{-1} corresponding to the **Cis-TS**. Visual inspection of the geometry and following of the IRC indicates that the decarboxylation mechanism is similar to that of **T3-TSa** as a dual hydrogen abstraction The water molecule releases a hydrogen to form H_2 and abstracts another hydrogen from the hydroxyl group. The transition state becomes a six member ring which greatly lowers the barrier height. Despite **C1** having the second highest binding energy of any complex presented in this study at 6.07 kcal mol^{-1}, the formation of the six member ring transition states immensely lowers the barrier to decarboxylation.

Inter1						
	HF	+δ MP2	+δ CCSD	+δ (T)	+δ T	NET
aug-cc-pVDZ	+6.04	–1.19	–0.28	–0.20	+0.01	[+4.38]
aug-cc-pVTZ	+6.05	–1.28	–0.24	–0.16	[+0.01]	[+4.38]
aug-cc-pVQZ	+6.11	–1.15	–0.21	–0.15	[+0.01]	[+4.60]
aug-cc-pV5Z	+6.15	–1.09	–0.20	–0.15	[+0.01]	[+4.72]
CBS LIMIT	[+6.18]	[–1.02]	[–0.20]	[–0.15]	[+0.01]	[+4.82]
$E_{CCSDT/CBS+\Delta}$ =4.82+0.43+0.37–0.04+0.03–0.01= **5.60**						
Inter2						
	HF	+δ MP2	+δ CCSD	+δ (T)	+δ T	NET
aug-cc-pVDZ	+8.26	–0.76	–0.53	–0.09	+0.00	[+6.88]
aug-cc-pVTZ	+8.61	–0.95	–0.48	–0.08	[+0.00]	[+7.10]
aug-cc-pVQZ	+8.66	–0.85	–0.44	–0.08	[+0.00]	[+7.28]
aug-cc-pV5Z	+8.69	–0.79	–0.43	–0.08	[+0.00]	[+7.39]
CBS LIMIT	[+8.71]	[–0.71]	[–0.43]	[–0.07]	[+0.00]	[+7.49]
$E_{CCSDT/CBS+\Delta}$ =7.49+0.44+0.37–0.02+0.02–0.01= **8.30**						

Table 6 Focal point analysis for all $H_2O\cdots FA$ interconversion transition states. The bold energy values are the $\Delta H_{0K} = \Delta E_{\mathrm{CCSDT/(CBS)}} + \Delta_{\mathrm{ZPVE}} + \Delta_{\mathrm{FC}} + \Delta_{.5(\mathrm{Q})} + \Delta_{\mathrm{Rel}} + \Delta_{\mathrm{DBOC}}$ energies relative to *trans*-FA plus H_2O in kcal mol^{-1}.

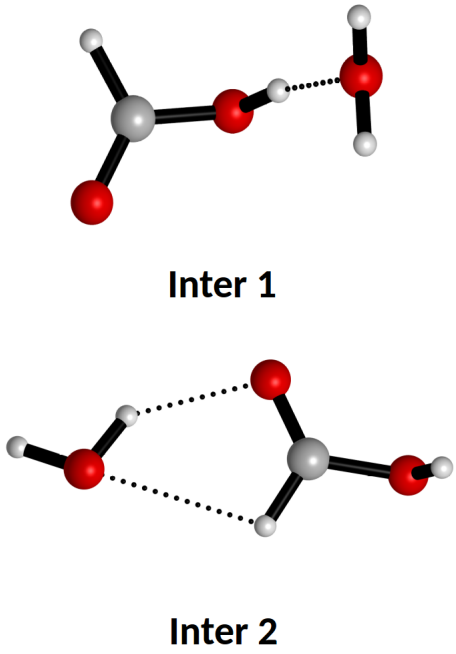

Fig. 5 The three water catalyzed interconversion transition states between the *trans* and *cis* conformers. Inter1 links C1 and T1. Inter2 links C2 and T2

3.5 Interconversions

Previous studies have indicated that the interconversion reaction between the *cis* and *trans* conformers may be relevant to regulating the decomposition pathways. There have been no theoretical studies published that have examined if water can play a role in the catalysis of this interconversion. We present two new transition states that link various *trans* and *cis* complexes via one a single transition state. Theoretically all wells can be connected

but this is an an exceedingly difficult task and beyond the scope of this work to identify all the connectivities. Both of these will be compared to the uncatalyzed transition state of formic acid **Inter** which has a barrier of 11.45 kcal mol^{-1}. The first is **Inter1** that links **C1** and **T1** via a transition state where the water molecule follows the hydroxyl group as it rotates and has a barrier of 12.97 kcal mol^{-1} and a vibrational mode of 379i cm^{-1}) (See Figure 5 and Table 6). **Inter2** is quite different and connects **T2** and **C2** via a transition state where the water is interacting with the carbonyl and α-hydrogen. This pathway proceeds through a vibrational mode of 618i, cm^{-1} and also has a relatively large barrier of 11.66 kcal mol^{-1}. Both interconversion transition states with an interacting water molecule are lower in energy than the uncatalyzed interconversion of formic acid. However, because the *trans*-FA$\cdots$H$_2$O complexes are also lowered in energy due to the presence of the water molecule none of the water catalyzed transition states lower the barrier to *trans* and *cis* interconversions and in fact **Inter1** greatly increases the barrier relative to **Inter**.

3.6 Kinetics

In order to quantify the catalytic importance of each FA$\cdots$H$_2$O conformer on the decomposition pathways, a simple kinetic model was utilized. Using a model similar to the one employed by Inaba[22], we use the canonical transition state theory to compute rate constants at various temperatures at the high pressure limit. Equation 6 describes the model which produces rate constants in units of s^{-1}. The asymmetric Eckart function was used to obtain tunneling factor (κ).[91,92] The q_{ts} and q_{complex} terms are the partition functions of the transition state and the FA$\cdots$H$_2$O complex (or just FA in the uncatalyzed case.), respectively. k_b is the Boltzman constant, T is the temperature, and h is Planks constant. The barrier to reaction is defined as E_{barrier}.

$$k = \kappa \frac{q_{\text{ts}}}{q_{\text{complex}}} \frac{k_b T}{h} \exp\left(-\frac{E_{\text{barrier}}}{k_b T}\right) \quad (6)$$

We note that the purpose of this model is to simply observe qualitative differences in decomposition rates for each water catalyzed pathway and compare them to the uncatalyzed decomposition, not necessarily to provide highly rigorous kinetics results. Additionally, we want to compare to the work of Inaba and determine how sensitive the reaction pathways are to conformation as opposed to number of water molecules.

The decarboxylation pathways have nearly identical rate constants relative to **Cis-TS** except for **C1-TS** which significantly increases the rate of reaction. At low temperatures **C1-TS** is more than four orders of magnitude faster than the other decarboxylation pathways while, the dehydration pathway rates show a bit more catalytic diversity. **Trans-TS**, **T2-TS**, and **T1-TS** all have very similar rates with **T1-TS** being the only decomposition route that is slightly slower than the uncatalyzed dehydration reaction which is most likely a consequence of the strongly bound **T1** binary complex. **T3-TSb** exhibits a slightly larger catalytic effect but is likely irrelevant as the **T3** complex will primarily proceed through the lower **T3-TSa** barrier. As was the case with **C1-TS**, the **T3-TSa** pathway significantly increases the rate of dehydra-

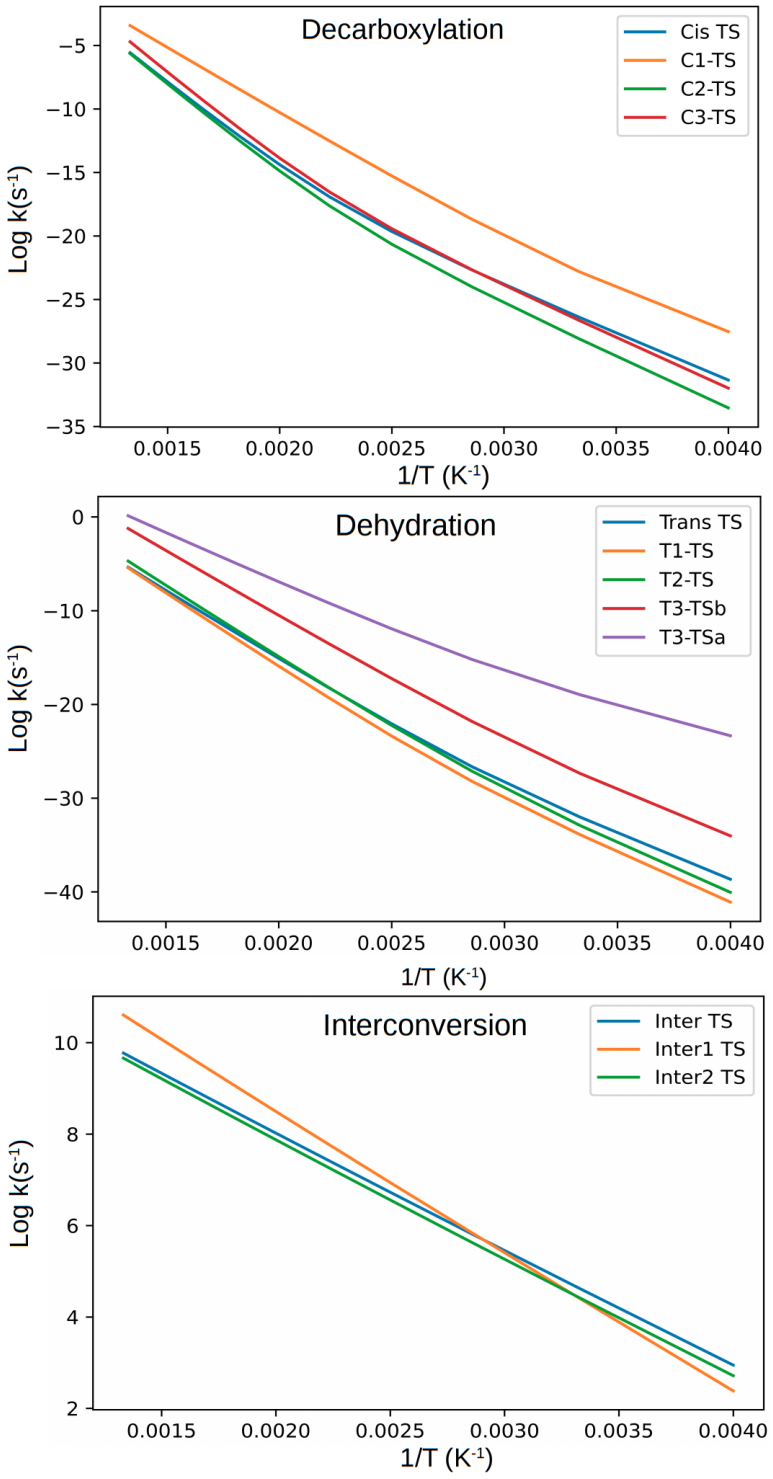

Fig. 6 Rate constants in units of Log(s^{-1}) for each decarboxylation, dehydration, and interconversion pathway as a function of inverse temperature.

tion relative to the **Trans-TS** pathway with a nearly 15 order of magnitude speedup making dehydration more favorable at low temperatures in the presence of a water molecule.

The interconversion reactions, as expected, are many orders of magnitude larger than either decomposition rate. The single water molecule has almost no catalytic influence on the FA interconversion and would have negligible impact on the equaillibrium ratio of the *trans* and *cis* isomers. In fact, **T1** has such a strong binding energy that **Inter1** is actually slightly slower at low temperatures than the uncatalyzed **Inter** process. The **Inter2** rate is essentially the same as **Inter** as well, so water has no discernible catalytic effect on the interconversion process.

Our kinetic data shows some clear results that elucidate the impact of formic acid dehydration and decarboxylation in the atmosphere. We confirm the fact that the specific conformers of $FA\cdots H_2O$ can play a significant role in lowering the barrier and increasing the rate of both of these processes, more so favoring dehydration. This is primarily due to the certain orientations allowing for an alternative mechanism to produce the same products as in **T3b-TS** and **C1-TS**. The effect of the other conformers on the overall rates has little significance and in certain cases (e.g. **T1-TS**) lowers the decomposition rates. We also note that the effect of additional water clusters as shown in the work of Inaba has a much larger catalytic effect than does changing the $FA\cdots H_2O$ complex structure. The water clusters are quite relevant due to the relatively high abundance of the water dimer in the atmosphere.[93] Our work does highlight that it is important to search for complexes that follow different lower energy paths to the same decomposition products. It may be the case that both catalytic effects could be capitalized on where multiple water molecules lower the decomposition barriers and also open the possibility to a diverse set of undiscovered conformers and mechanisms.

Overall, the decomposition of FA following the decarboxylation and dehydration pathways are likely too slow to significantly impact atmospheric concentrations. Even though the various $FA\cdots H_2O$ complexes can significantly lower the barrier, it is likely still too small to influence the atmospheric FA budget in a significant way. Prior research has found that atmospheric FA has a lifetime of approximately 3.2 days and is primarily removed by wet and dry decomposition, photochemical oxidation, and reaction with the OH radical all of which are faster than formic acid decomposition rates even in the presence of water.[94–97] For example, the rate of reaction for FA with the OH radical is 3.2×10^{-13} cm^3 $molecules^{-1}$ s^{-1}[95,96] at atmospheric conditions which corresponds to residence times of at least a week. The dry and wet deposition mechanisms are expected to be even faster than this indicating that the these processes will dominate compared to FA water catalyzed decomposition.[97] By comparison, even at 298 K, the largest rates of reaction for the water catalyzed decarboxylation and dehydration are approximately on the order of only 10^{-15} s^{-1} and 10^{-20} s^{-1}, respectively.

4 Conclusions

The research we present provides novel insights into the noncovalent complexes formed between formic acid and a single water molecule. We also examine the catalytic effect of a water molecule on formic acid decomposition and isomerization, taking into consideration all possible conformations which had not been done before. Our work characterized three *trans*-$FA\cdots H_2O$ and four *cis*-$FA\cdots H_2O$ complexes, of which **C3** is entirely new to the literature. We computed highly reliable geometries and harmonic vibrational frequencies at the CCSD(T)/aug-cc-pVTZ level of theory and binding energies ranging from 2.02 to 7.37 kcal mol^{-1} and 2.55 to 6.07 kcal mol^{-1} at the CCSDT(Q)/CBS level of theory for the *cis* and *trans* complexes, respectively. Each complex was further examined by NBO analysis. Our research also includes the first characterization of water catalyzed isomerization reactions (between *trans*-FA and *cis*-FA).

Our research thoroughly describes the catalytic effect of a single water molecule on the decomposition mechanisms of formic acid. We find that a single water molecule catalysis favors the dehydration pathway, agreeing with experiment, but cannot catalyze any decomposition mechanism to be competitive enough with the other processes that remove FA in the atmosphere. Additionally, considering all conformers at best results in a fifteen order of magnitude increase at low temperatures in the rate of decomposition, but this is less than the catalytic effect of larger water clusters presented in previous work. We find that due to the strong $FA\cdots H_2O$ interactions, that there is no water assisted interconversion pathway that is significantly faster than the the uncatalyzed interconversion, therefore a single water molecule will not influence the ratio of *trans*-Fa to *cis*-FA in the atmosphere. We do highlight two very important findings that may guide similar studies on the catalytic effect of noncovalent binary complexes. 1) In the case of **C1-TS** and **T3-TSa**, the presence of a water molecule allows for alternate decomposition mechanisms via ring-like transition states that greatly lower the barriers to 49.66 kcal mol^{-1} and 50.97 kcal mol^{-1} for decarboxylation and dehydration, respectively. This demonstrates the importance of considering alternate reaction pathways which likely become more complicated in the presence of more than one small noncovalent catalyst. 2) We found that **T3** can proceed through a dehydration mechanism similar to the uncatalyzed dehydration process (**T3-TSb**) and the alternate ring-like transition state previously mentioned (**T3-TSa**). The difference in barrier heights between the two transition states is 13.22 kcal mol^{-1} indicating how important it is to correctly characterize all transition states that may be accessible to a given binary complex. We hope that this work can serve as a rigorous benchmark of the ubiquitous $FA\cdots H_2O$ system and help guide future work on other similar atmospheric reactions.

Conflicts of interest

There are no conflicts to declare.

Acknowledgements

This work was supported by U.S. National Science Foundation under grant number CHE-1661604. MEW wishes to dedicate this to his beautiful bride Morgan.

Notes and references

1 J. M. Anglada, M. Martins-Costa, J. S. Francisco and M. F. Ruiz-López, *Acc. Chem. Res.*, 2015, **48**, 575–583.

2 M. Jerrett, *Nature*, 2015, **525**, 330–331.

3 M. Kulmala, *Nature*, 2015, **526**, 497–499.

4 S. Tanaka, *J. Health Econ.*, 2015, **42**, 90–103.

5 M. S. Kamal, S. A. Razzak and M. M. Hossain, *Atmos. Environ.*, 2016, **140**, 117–134.

6 M. Glasius and A. H. Goldstein, *Environ. Sci. Technol.*, 2016, **50**, 2754–2764.

7 B. Nozière, M. Kalberer, M. Claeys, J. Allan, B. D'Anna, S. Decesari, E. Finessi, M. Glasius, I. Grgić, J. F. Hamilton, T. Hoffmann, Y. Iinuma, M. Jaoui, A. Kahnt, C. J. Kampf, I. Kourtchev, W. Maenhaut, N. Marsden, S. Saarikoski, J. Schnelle-Kreis, J. D. Surratt, S. Szidat, R. Szmigielski and A. Wisthaler, *Chem. Rev.*, 2015, **115**, 3919–3983.

8 R. Zhang, A. Khalizov, L. Wang, M. Hu and W. Xu, *Chem. Rev.*, 2012, **112**, 1957–2011.

9 D. A. Knopf, P. A. Alpert and B. Wang, *ACS Earth Space Chem.*, 2018, **2**, 168–202.

10 R. Zhang, I. Suh, J. Zhao, D. Zhang, E. C. Fortner, X. Tie, L. T. Molina and M. J. Molina, *Science*, 2004, **304**, 1487–1490.

11 S. Chaliyakunnel, D. Millet, K. Wells, K. Cady-Pereira and M. Shephard, *Environ. Sci. Technol.*, 2016, **50**, 5631–5640.

12 K. Azuma, I. Uchiyama, S. Uchiyama and N. Kunugita, *Environ. Res.*, 2016, **145**, 39–49.

13 D. B. Millet, M. Baasandorj, D. K. Farmer, J. A. Thornton, K. Baumann, P. Brophy, S. Chaliyakunnel, J. A. de Gouw, M. Graus, L. Hu, A. Koss, B. H. Lee, F. D. Lopez-Hilfiker, J. A. Neuman, F. Paulot, J. Peischl, I. B. Pollack, T. B. Ryerson, C. Warneke, B. J. Williams and J. Xu, *Atmos. Chem. Phys.*, 2015, **15**, 6283–6304.

14 A. Chebbi and P. Carlier, *Atmos. Environ.*, 1996, **30**, 4233–4249.

15 T. Stavrakou, J.-F. Müller, J. Peeters, A. Razavi, L. Clarisse, C. Clerbaux, P.-F. Coheur, D. Hurtmans, M. D. Mazière, C. Vigouroux, N. M. Deutscher, D. W. T. Griffith, N. Jones and C. Paton-Walsh, *Nature Geosci*, 2012, **5**, 26–30.

16 A. T. Archibald, A. S. Petit, C. J. Percival, J. N. Harvey and D. E. Shallcross, *Atmos. Sci. Lett.*, 2009, **10**, 102–108.

17 D. U. Andrews, B. R. Heazlewood, A. T. Maccarone, T. Conroy, R. J. Payne, M. J. T. Jordan and S. H. Kable, *Science*, 2012, **337**, 1203–1206.

18 W. H. Hocking, *Zeitschrift für Naturforschung A*, 2014, **31**, 1113–1121.

19 A. Aerts, P. Carbonnière, F. Richter and A. Brown, *J. Chem. Phys.*, 2020, **152**, 024305.

20 N. Akiya and P. E. Savage, *AIChE Journal*, 1998, **44**, 405–415.

21 G. d. S. Machado, E. M. Martins, L. Baptista and G. F. Bauerfeldt, *Int. J. Chem. Kinet.*, 2020, **52**, 188–196.

22 S. Inaba, *J. Phys. Chem. A*, 2014, **118**, 3026–3038.

23 S.-W. Hu, X.-Y. Wang, T.-W. Chu and X.-Q. Liu, *J. Phys. Chem. A*, 2005, **109**, 9129–9140.

24 L. George and W. Sander, *Spectrochim. Acta A*, 2004, **60**, 3225–3232.

25 D. Priem, T.-K. Ha and A. Bauder, *J. Chem. Phys.*, 2000, **113**, 169–175.

26 M. Rozenberg, A. Loewenschuss and C. J. Nielsen, *J. Phys. Chem. A*, 2015, **119**, 8497–8502.

27 K. Marushkevich, L. Khriachtchev and M. Räsänen, *J. Phys. Chem. A*, 2007, **111**, 2040–2042.

28 J. W. Keller, B. L. Harrod and S. A. Chowdhury, *J. Phys. Chem. A*, 2010, **114**, 13182–13188.

29 L. Yuxiu Li, N. A. Seifert, F. Xie, M. Heger, Y. Xu and W. Jäger, *Phys. Chem. Chem. Phys.*, 2018, **20**, 21345–21351.

30 M. Torrent-Sucarrat and J. M. Anglada, *Chem. Phys. Chem.*, 2004, **5**, 183–191.

31 M. Torrent-Sucarrat and J. M. Anglada, *J. Phys. Chem. A*, 2006, **110**, 9718–9726.

32 C. Qu and J. M. Bowman, *Phys. Chem. Chem. Phys.*, 2016, **18**, 24835–24840.

33 E. Miliordos and S. S. Xantheas, *The J. Chem. Phys.*, 2015, **142**, 094311.

34 L. Spada, Q. Gou, B. M. Giuliano and W. Caminati, *J. Phys. Chem. A*, 2016, **120**, 5094–5098.

35 G. Karir, G. Kumar, B. P. Kar and K. S. Viswanathan, *J. Phys. Chem. A*, 2018, **122**, 2046–2059.

36 L. Evangelisti, L. Spada, W. Li, A. Ciurlini, J.-U. Grabow and W. Caminati, *J. Phys. Chem. A*, 2016, **120**, 2863–2867.

37 L. Evangelisti, L. Spada, W. Li, S. Blanco, J. Carlos López, A. Lesarri, J.-U. Grabow and W. Caminati, *Phys. Chem. Chem. Phys.*, 2017, **19**, 204–209.

38 Y. Jin, J. Wang, Q. Gou, Z. Xia and G. Feng, *Spectrochim. Acta A*, 2019, **206**, 185–189.

39 R. B. Mackenzie, C. T. Dewberry and K. R. Leopold, *J. Phys. Chem. A*, 2016, **120**, 2268–2273.

40 J. J. Panek, P. K. Wawrzyniak, Z. Latajka and J. Lundell, *Chem. Phys. Lett.*, 2006, **417**, 100–104.

41 E. Sánchez-García, M. Studentkowski, L. A. Montero and W. Sander, *Chem. Phys. Chem.*, 2005, **6**, 618–624.

42 E. Sánchez-García, A. Mardyukov, M. Studentkowski, L. A. Montero and W. Sander, *J. Phys. Chem. A*, 2006, **110**, 13775–13785.

43 E. Sánchez-García, L. George, L. A. Montero and W. Sander, *J. Phys. Chem. A*, 2004, **108**, 11846–11854.

44 H.-T. Chen, J.-G. Chang and H.-L. Chen, *J. Phys. Chem. A*, 2008, **112**, 8093–8099.

45 P. Åstrand, G. Karlström, A. Engdahl and B. Nelander, *J. Chem. Phys.*, 1995, **102**, 3534–3554.

46 P. R. Rablen, J. W. Lockman and W. L. Jorgensen, *J. Phys. Chem. A*, 1998, **102**, 3782–3797.

47 Z. Zhou, Y. Shi and X. Zhou, *J. Phys. Chem. A*, 2004, **108**, 813–822.

48 A. Elwardany, E. F. Nasir, E. Es-sebbar and A. Farooq, *P. Combust. Inst.*, 2015, **35**, 429–436.

49 R. M. Vichietti, R. F. K. Spada, A. B. F. d. Silva, F. B. C. Machado and R. L. A. Haiduke, *Chem. Select*, 2017, **2**, 7267–

7272.
50 S. C. Moldoveanu, *Techniques and Instrumentation in Analytical Chemistry*, Elsevier, 2010, vol. 28, pp. 471–526.
51 J. S. Francisco, *J. Chem. Phys.*, 1992, **96**, 1167–1175.
52 J.-G. Chang, H.-T. Chen, S. Xu and M. C. Lin, *J. Phys. Chem. A*, 2007, **111**, 6789–6797.
53 P. G. Blake and C. N. Hinshelwood, *P. Roy. Soc. Lond. A Mat.*, 1960, **255**, 444–455.
54 T. Ida, M. Nishida and Y. Hori, *J. Phys. Chem. A*, 2019, **123**, 9579–9586.
55 K. Saito, T. Shiose, O. Takahashi, Y. Hidaka, F. Aiba and K. Tabayashi, *J. Phys. Chem. A*, 2005, **109**, 5352–5357.
56 P. Ruelle, U. W. Kesselring and . Ho Nam-Tran, *J. Am. Chem. Soc.*, 1986, **108**, 371–375.
57 K. Saito, T. Kakumoto, H. Kuroda, S. Torii and A. Imamura, *J. Chem. Phys.*, 1984, **80**, 4989–4996.
58 J. D. Goddard, Y. Yamaguchi and H. F. Schaefer, *J. Chem. Phys.*, 1992, **96**, 1158–1166.
59 P. Pracht, F. Bohle and S. Grimme, *Phys. Chem. Chem. Phys.*, 2020, **22**, 7169–7192.
60 T. H. Dunning, *J. Chem. Phys.*, 1989, **90**, 1007–1023.
61 I. Shavitt and R. J. Bartlett, *Many-Body Methods in Chemistry and Physics: MBPT and Coupled-Cluster Theory*, Cambridge University Press, 2009.
62 R. J. Bartlett, J. D. Watts, S. A. Kucharski and J. Noga, *Chem. Phys. Letters*, 1990, **165**, 513–522.
63 J. F. Stanton, *Chem. Phys. Letters*, 1997, **281**, 130–134.
64 K. Raghavachari, G. W. Trucks, J. A. Pople and M. Head-Gordon, *Chem. Phys. Letters*, 1989, **157**, 479–483.
65 J. F. Stanton, J. Gauss, L. Cheng, M. E. Harding, D. A. Matthews and P. G. Szalay, *CFOUR, Coupled-Cluster techniques for Computational Chemistry, a quantum-chemical program package*, With contributions from A.A. Auer, R.J. Bartlett, U. Benedikt, C. Berger, D.E. Bernholdt, Y.J. Bomble, O. Christiansen, F. Engel, R. Faber, M. Heckert, O. Heun, M. Hilgenberg, C. Huber, T.-C. Jagau, D. Jonsson, J. Jusélius, T. Kirsch, K. Klein, W.J. Lauderdale, F. Lipparini, T. Metzroth, L.A. Mück, D.P. O'Neill, D.R. Price, E. Prochnow, C. Puzzarini, K. Ruud, F. Schiffmann, W. Schwalbach, C. Simmons, S. Stopkowicz, A. Tajti, J. Vázquez, F. Wang, J.D. Watts and the integral packages MOLECULE (J. Almlöf and P.R. Taylor), PROPS (P.R. Taylor), ABACUS (T. Helgaker, H.J. Aa. Jensen, P. Jørgensen, and J. Olsen), and ECP routines by A. V. Mitin and C. van Wüllen. For the current version, see http://www.cfour.de.
66 R. M. Parrish, L. A. Burns, D. G. A. Smith, A. C. Simmonett, A. E. DePrince, E. G. Hohenstein, U. Bozkaya, A. Y. Sokolov, R. Di Remigio, R. M. Richard, J. F. Gonthier, A. M. James, H. R. McAlexander, A. Kumar, M. Saitow, X. Wang, B. P. Pritchard, P. Verma, H. F. Schaefer, K. Patkowski, R. A. King, E. F. Valeev, F. A. Evangelista, J. M. Turney, T. D. Crawford and C. D. Sherrill, *J. Chem. Theory Comput.*, 2017, **13**, 3185–3197.
67 M. S. Schuurman, S. R. Muir, W. D. Allen and H. F. Schaefer, *J. Chem. Phys.*, 2004, **120**, 11586–11599.
68 J. M. Gonzales, C. Pak, R. S. Cox, W. D. Allen, H. F. Schaefer, A. G. Csaszar and G. Tarczay, *Chem. Eur. J.*, 2003, **9**, 2173–2192.
69 A. G. Császár, W. D. Allen and H. F. Schaefer, *J. Chem. Phys.*, 1998, **108**, 9751–9764.
70 A. L. L. East and W. D. Allen, *J. Chem. Phys.*, 1993, **99**, 4638–4650.
71 G. J. R. Aroeira, A. S. Abbott, S. N. Elliott, J. M. Turney and H. F. Schaefer, *Phys. Chem. Chem. Phys.*, 2019, **21**, 17760–17771.
72 M. M. Davis, J. D. Weidman, A. S. Abbott, G. E. Douberly, J. M. Turney and H. F. Schaefer, *J. Chem. Phys.*, 2019, **151**, 124302.
73 D. Feller, K. A. Peterson and T. D. Crawford, *J. Chem. Phys.*, 2006, **124**, 054107.
74 T. Helgaker, W. Klopper, H. Koch and J. Noga, *J. Chem. Phys.*, 1997, **106**, 9639–9646.
75 H.-J. Werner, P. J. Knowles, G. Knizia, F. R. Manby and M. Schütz, *WIREs Comput Mol Sci*, 2012, **2**, 242–253.
76 K. A. Peterson and T. H. Dunning, *J. Chem. Phys.*, 2002, **117**, 10548–10560.
77 P. Verma, W. D. Derricotte and F. A. Evangelista, *J. Chem. Theory Comput.*, 2016, **12**, 144–156.
78 H. Sellers and P. Pulay, *Chem. Phys. Letters*, 1984, **103**, 463–465.
79 N. C. Handy and H. F. Yamaguchi, Yukio and, *Journal of Chem. Phys.*, 1986, **84**, 4481.
80 J. Noga and R. J. Bartlett, *J. Chem. Phys.*, 1987, **86**, 7041–7050.
81 G. E. Scuseria and H. F. Schaefer, *Chem. Phys. Letters*, 1988, **152**, 382–386.
82 Y. J. Bomble, J. F. Stanton, M. Kállay and J. Gauss, *J. Chem. Phys.*, 2005, **123**, 054101.
83 M. Kállay and J. Gauss, *J. Chem. Phys.*, 2008, **129**, 144101.
84 T. Clark, J. Chandrasekhar, G. W. Spitznagel and P. V. R. Schleyer, *J. Comput. Chem.*, 1983, **4**, 294–301.
85 P. C. Hariharan and J. A. Pople, *Theoret. Chim. Acta*, 1973, **28**, 213–222.
86 W. J. Hehre, R. Ditchfield and J. A. Pople, *J. Chem. Phys.*, 1972, **56**, 2257–2261.
87 E. D. Glendening, C. R. Landis and F. Weinhold, *Wires. Comput. Mol. Sci.*, 2012, **2**, 1–42.
88 E. D. Glendening, C. R. Landis and F. Weinhold, *J. Comput. Chem.*, 2013, **34**, 1429–1437.
89 F. Neese, *Wires. Comput. Mol. Sci.*, 2012, **2**, 73–78.
90 A. D. Becke, *J. Chem. Phys.*, 1993, **98**, 5648–5652.
91 J. Espinosa-García, F. J. Olivares del Valle and J. C. Corchado, *Chemical Physics*, 1994, **183**, 95–100.
92 H. S. Johnston and J. Heicklen, *The Journal of Physical Chemistry*, 1962, **66**, 532–533.
93 M. Y. Tretyakov, M. A. Koshelev, E. A. Serov, V. V. Parshin, T. A. Odintsova and G. M. Bubnov, *Physics-Uspekhi*, 2014, **57**, 1083.
94 D. Grosjean, *Atmospheric Environment. Part A. General Topics*, 1992, **26**, 3279–3286.

95 Z. C and S. F, *Physico-Chemical Behaviour of Atmospheric Pollutants*, 1982, 129–137.

96 E. Sanhueza, L. Figueroa and M. Santana, *Atmospheric Environment*, 1996, **30**, 1861–1873.

97 F. Paulot, D. Wunch, J. D. Crounse, G. C. Toon, D. B. Millet, P. F. DeCarlo, C. Vigouroux, N. M. Deutscher, G. González Abad, J. Notholt, T. Warneke, J. W. Hannigan, C. Warneke, J. A. de Gouw, E. J. Dunlea, M. De Mazière, D. W. T. Griffith, P. Bernath, J. L. Jimenez and P. O. Wennberg, *Atmospheric Chemistry and Physics*, 2011, **11**, 1989–2013.